Observation of $J/\psi p$ Resonances Consistent with Pentaquark States in $\Lambda_b^0 \to J/\psi K^- p$ Decays

R. Aaij *et al.*[*]
(LHCb Collaboration)

(Received 13 July 2015; published 12 August 2015)

Observations of exotic structures in the $J/\psi p$ channel, which we refer to as charmonium-pentaquark states, in $\Lambda_b^0 \to J/\psi K^- p$ decays are presented. The data sample corresponds to an integrated luminosity of 3 fb^{-1} acquired with the LHCb detector from 7 and 8 TeV pp collisions. An amplitude analysis of the three-body final state reproduces the two-body mass and angular distributions. To obtain a satisfactory fit of the structures seen in the $J/\psi p$ mass spectrum, it is necessary to include two Breit-Wigner amplitudes that each describe a resonant state. The significance of each of these resonances is more than 9 standard deviations. One has a mass of $4380 \pm 8 \pm 29$ MeV and a width of $205 \pm 18 \pm 86$ MeV, while the second is narrower, with a mass of $4449.8 \pm 1.7 \pm 2.5$ MeV and a width of $39 \pm 5 \pm 19$ MeV. The preferred J^P assignments are of opposite parity, with one state having spin $3/2$ and the other $5/2$.

DOI: 10.1103/PhysRevLett.115.072001 PACS numbers: 14.40.Pq, 13.25.Gv

Introduction and summary.—The prospect of hadrons with more than the minimal quark content ($q\bar{q}$ or qqq) was proposed by Gell-Mann in 1964 [1] and Zweig [2], followed by a quantitative model for two quarks plus two antiquarks developed by Jaffe in 1976 [3]. The idea was expanded upon [4] to include baryons composed of four quarks plus one antiquark; the name pentaquark was coined by Lipkin [5]. Past claimed observations of pentaquark states have been shown to be spurious [6], although there is at least one viable tetraquark candidate, the $Z(4430)^+$ observed in $\bar{B}^0 \to \psi' K^- \pi^+$ decays [7–9], implying that the existence of pentaquark baryon states would not be surprising. States that decay into charmonium may have particularly distinctive signatures [10].

Large yields of $\Lambda_b^0 \to J/\psi K^- p$ decays are available at LHCb and have been used for the precise measurement of the Λ_b^0 lifetime [11]. (In this Letter, mention of a particular mode implies use of its charge conjugate as well.) This decay can proceed by the diagram shown in Fig. 1(a), and is expected to be dominated by $\Lambda^* \to K^- p$ resonances, as are evident in our data shown in Fig. 2(a). It could also have exotic contributions, as indicated by the diagram in Fig. 1(b), which could result in resonant structures in the $J/\psi p$ mass spectrum shown in Fig. 2(b).

In practice, resonances decaying strongly into $J/\psi p$ must have a minimal quark content of $c\bar{c}uud$, and thus are charmonium pentaquarks; we label such states P_c^+, irrespective of the internal binding mechanism. In order to ascertain if the structures seen in Fig. 2(b) are resonant in nature and not due to reflections generated by the Λ^* states, it is necessary to perform a full amplitude analysis, allowing for interference effects between both decay sequences.

The fit uses five decay angles and the $K^- p$ invariant mass m_{Kp} as independent variables. First, we tried to fit the data with an amplitude model that contains 14 Λ^* states listed by the Particle Data Group [12]. As this did not give a satisfactory description of the data, we added one P_c^+ state, and when that was not sufficient we included a second state. The two P_c^+ states are found to have masses of $4380 \pm 8 \pm 29$ MeV and $4449.8 \pm 1.7 \pm 2.5$ MeV, with corresponding widths of $205 \pm 18 \pm 86$ MeV and $39 \pm 5 \pm 19$ MeV. (Natural units are used throughout this Letter. Whenever two uncertainties are quoted, the first is statistical and the second systematic.) The fractions of the total sample due to the lower mass and higher mass states are $(8.4 \pm 0.7 \pm 4.2)\%$ and $(4.1 \pm 0.5 \pm 1.1)\%$, respectively. The best fit solution has spin-parity J^P values of $(3/2^-, 5/2^+)$. Acceptable solutions are also found for additional cases with opposite parity, either $(3/2^+, 5/2^-)$ or $(5/2^+, 3/2^-)$. The best fit projections are shown in Fig. 3. Both m_{Kp} and the peaking structure in $m_{J/\psi p}$ are reproduced by the fit. The significances of the lower mass and

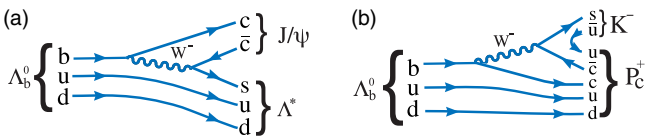

FIG. 1 (color online). Feynman diagrams for (a) $\Lambda_b^0 \to J/\psi \Lambda^*$ and (b) $\Lambda_b^0 \to P_c^+ K^-$ decay.

[*]Full author list given at end of the article.

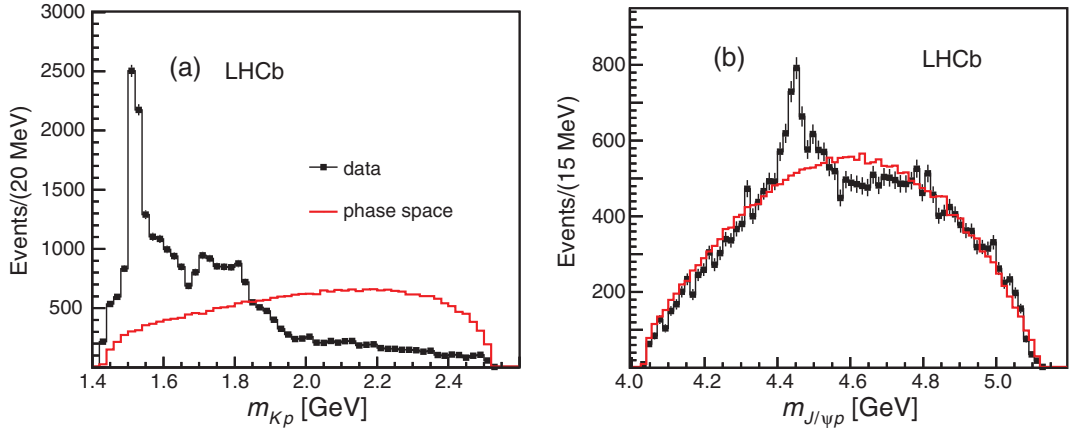

FIG. 2 (color online). Invariant mass of (a) K^-p and (b) $J/\psi p$ combinations from $\Lambda_b^0 \to J/\psi K^- p$ decays. The solid (red) curve is the expectation from phase space. The background has been subtracted.

higher mass states are 9 and 12 standard deviations, respectively.

Analysis and results.—We use data corresponding to 1 fb^{-1} of integrated luminosity acquired by the LHCb experiment in pp collisions at 7 TeV center-of-mass energy, and 2 fb^{-1} at 8 TeV. The LHCb detector [13] is a single-arm forward spectrometer covering the pseudorapidity range, $2 < \eta < 5$. The detector includes a high-precision tracking system consisting of a silicon-strip vertex detector surrounding the pp interaction region [14], a large-area silicon-strip detector located upstream of a dipole magnet with a bending power of about 4 Tm, and three stations of silicon-strip detectors and straw drift tubes [15] placed downstream of the magnet. Different types of charged hadrons are distinguished using information from two ring-imaging Cherenkov detectors [16]. Muons are identified by a system composed of alternating layers of iron and multiwire proportional chambers [17].

Events are triggered by a $J/\psi \to \mu^+\mu^-$ decay, requiring two identified muons with opposite charge, each with transverse momentum, p_T, greater than 500 MeV. The dimuon system is required to form a vertex with a fit $\chi^2 < 16$, to be significantly displaced from the nearest pp interaction vertex, and to have an invariant mass within 120 MeV of the J/ψ mass [12]. After applying these requirements, there is a large J/ψ signal over a small background [18]. Only candidates with dimuon invariant mass between -48 and $+43$ MeV relative to the observed J/ψ mass peak are selected, the asymmetry accounting for final-state electromagnetic radiation.

Analysis preselection requirements are imposed prior to using a gradient boosted decision tree, BDTG [19], that separates the Λ_b^0 signal from backgrounds. Each track is required to be of good quality and multiple reconstructions of the same track are removed. Requirements on the individual particles include $p_T > 550$ MeV for muons,

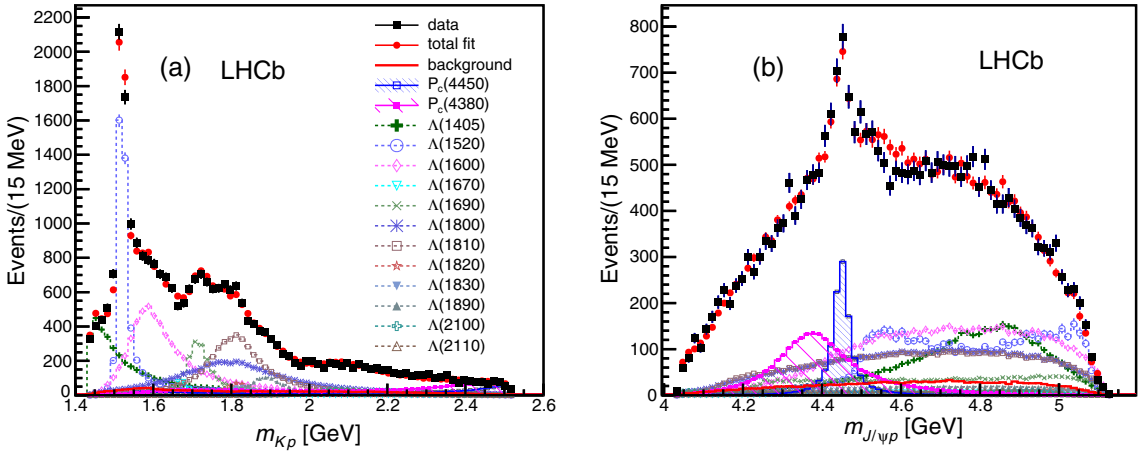

FIG. 3 (color online). Fit projections for (a) m_{Kp} and (b) $m_{J/\psi p}$ for the reduced Λ^* model with two P_c^+ states (see Table I). The data are shown as solid (black) squares, while the solid (red) points show the results of the fit. The solid (red) histogram shows the background distribution. The (blue) open squares with the shaded histogram represent the $P_c(4450)^+$ state, and the shaded histogram topped with (purple) filled squares represents the $P_c(4380)^+$ state. Each Λ^* component is also shown. The error bars on the points showing the fit results are due to simulation statistics.

and $p_T > 250$ MeV for hadrons. Each hadron must have an impact parameter χ^2 with respect to the primary pp interaction vertex larger than 9, and must be positively identified in the particle identification system. The K^-p system must form a vertex with $\chi^2 < 16$, as must the two muons from the J/ψ decay. Requirements on the Λ_b^0 candidate include a vertex $\chi^2 < 50$ for 5 degrees of freedom, and a flight distance of greater than 1.5 mm. The vector from the primary vertex to the Λ_b^0 vertex must align with the Λ_b^0 momentum so that the cosine of the angle between them is larger than 0.999. Candidate $\mu^+\mu^-$ combinations are constrained to the J/ψ mass for subsequent use in event selection.

The BDTG technique involves a "training" procedure using sideband data background and simulated signal samples. (The variables used are listed in the Supplemental Material [20].) We use 2×10^6 $\Lambda_b^0 \to J/\psi K^- p$ events with $J/\psi \to \mu^+\mu^-$ that are generated uniformly in phase space in the LHCb acceptance, using PYTHIA [21] with a special LHCb parameter tune [22], and the LHCb detector simulation based on GEANT4 [23], described in Ref. [24]. The product of the reconstruction and trigger efficiencies within the LHCb geometric acceptance is about 10%. In addition, specific backgrounds from $\bar{B}_s^0$ and $\bar{B}^0$ decays are vetoed. This is accomplished by removing combinations that when interpreted as $J/\psi K^+K^-$ fall within ± 30 MeV of the $\bar{B}_s^0$ mass or when interpreted as $J/\psi K^-\pi^+$ fall within ± 30 MeV of the $\bar{B}^0$ mass. This requirement effectively eliminates background from these sources and causes only smooth changes in the detection efficiencies across the Λ_b^0 decay phase space. Backgrounds from Ξ_b decays cannot contribute significantly to our sample. We choose a relatively tight cut on the BDTG output variable that leaves $26\,007 \pm 166$ signal candidates containing 5.4% background within ± 15 MeV ($\pm 2\sigma$) of the $J/\psi K^- p$ mass peak, as determined by the unbinned extended likelihood fit shown in Fig. 4. The combinatorial background is modeled with an exponential function and the Λ_b^0 signal shape is parametrized by a double-sided Hypatia function [25], where the signal radiative tail parameters are fixed to values obtained from simulation. For subsequent analysis we constrain the $J/\psi K^- p$ four-vectors to give the Λ_b^0 invariant mass and the Λ_b^0 momentum vector to be aligned with the measured direction from the primary to the Λ_b^0 vertices [26].

In Fig. 5 we show the "Dalitz" plot [27] using the K^-p and $J/\psi p$ invariant masses-squared as independent variables. A distinct vertical band is observed in the K^-p invariant mass distribution near 2.3 GeV^2 corresponding to the $\Lambda(1520)$ resonance. There is also a distinct horizontal band near 19.5 GeV^2. As we see structures in both K^-p and $J/\psi p$ mass distributions we perform a full amplitude analysis, using the available angular variables in addition to the mass distributions, in order to determine the resonances present. No structure is seen in the $J/\psi K^-$ invariant mass.

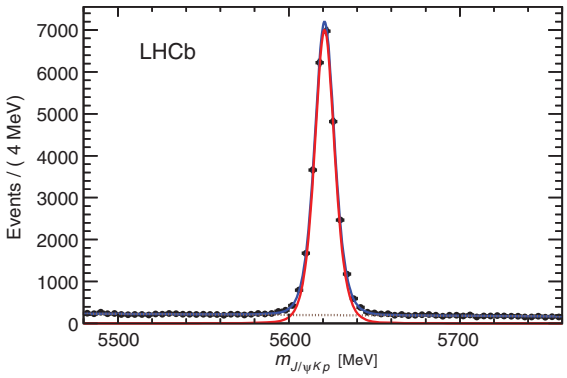

FIG. 4 (color online). Invariant mass spectrum of $J/\psi K^- p$ combinations, with the total fit, signal, and background components shown as solid (blue), solid (red), and dashed lines, respectively.

We consider the two interfering processes shown in Fig. 1, which produce two distinct decay sequences: $\Lambda_b^0 \to J/\psi \Lambda^*$, $\Lambda^* \to K^- p$ and $\Lambda_b^0 \to P_c^+ K^-$, $P_c^+ \to J/\psi p$, with $J/\psi \to \mu^+\mu^-$ in both cases. We use the helicity formalism [28] in which each sequential decay $A \to BC$ contributes to the amplitude a term

$$\mathcal{H}^{A\to BC}_{\lambda_B,\lambda_C} D^{J_A}_{\lambda_A,\lambda_B-\lambda_C}(\phi_B,\theta_A,0)^* R_A(m_{BC}) = \mathcal{H}^{A\to BC}_{\lambda_B,\lambda_C} e^{i\lambda_A\phi_B} d^{J_A}_{\lambda_A,\lambda_B-\lambda_C}(\theta_A) R_A(m_{BC}), \quad (1)$$

where λ is the quantum number related to the projection of the spin of the particle onto its momentum vector (helicity) and $\mathcal{H}^{A\to BC}_{\lambda_B,\lambda_C}$ are complex helicity-coupling amplitudes describing the decay dynamics. Here, θ_A and ϕ_B are the polar and azimuthal angles of B in the rest frame of A (θ_A is known as the "helicity angle" of A). The three arguments of Wigner's D matrix are Euler angles describing the rotation of the initial coordinate system with the z axis along the

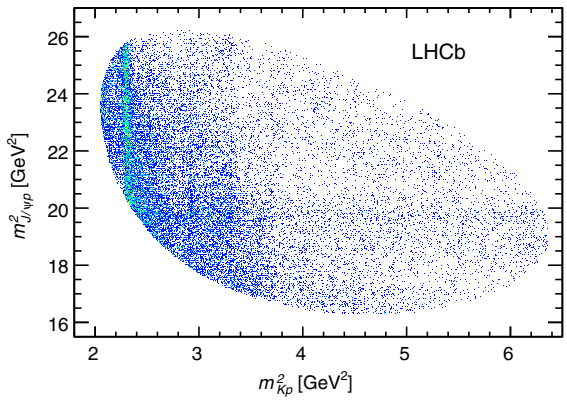

FIG. 5 (color online). Invariant mass squared of K^-p versus $J/\psi p$ for candidates within ± 15 MeV of the Λ_b^0 mass.

helicity axis of A to the coordinate system with the z axis along the helicity axis of B [12]. We choose the convention in which the third Euler angle is zero. In Eq. (1), $d^{J_A}_{\lambda_A,\lambda_B-\lambda_C}(\theta_A)$ is the Wigner small-d matrix. If A has a non-negligible natural width, the invariant mass distribution of the B and C daughters is described by the complex function $R_A(m_{BC})$ discussed below; otherwise $R_A(m_{BC}) = 1$.

Using Clebsch-Gordan coefficients, we express the helicity couplings in terms of LS couplings ($B_{L,S}$), where L is the orbital angular momentum in the decay, and S is the total spin of A plus B:

$$\mathcal{H}^{A\to BC}_{\lambda_B,\lambda_C} = \sum_L \sum_S \sqrt{\frac{2L+1}{2J_A+1}} B_{L,S} \begin{pmatrix} J_B & J_C \\ \lambda_B & -\lambda_C \end{pmatrix} \begin{pmatrix} S \\ \lambda_B-\lambda_C \end{pmatrix} \times \begin{pmatrix} L & S \\ 0 \;\; \lambda_B-\lambda_C \end{pmatrix} \begin{pmatrix} J_A \\ \lambda_B-\lambda_C \end{pmatrix}, \quad (2)$$

where the expressions in parentheses are the standard Wigner $3j$ symbols. For strong decays, possible L values are constrained by the conservation of parity (P): $P_A = P_B P_C (-1)^L$.

Denoting J/ψ as ψ, the matrix element for the $\Lambda_b^0 \to J/\psi\Lambda^*$ decay sequence is

$$\mathcal{M}^{\Lambda^*}_{\lambda_{\Lambda_b^0},\lambda_p,\Delta\lambda_\mu} \equiv \sum_n \sum_{\lambda_{\Lambda^*}} \sum_{\lambda_\psi} \mathcal{H}^{\Lambda_b^0\to\Lambda_n^*\psi}_{\lambda_{\Lambda^*},\lambda_\psi} D^{1/2}_{\lambda_{\Lambda_b^0},\lambda^*_\Lambda-\lambda_\psi}(0,\theta_{\Lambda_b^0},0)^* \times \mathcal{H}^{\Lambda_n^*\to Kp}_{\lambda_p,0} D^{J_{\Lambda_n^*}}_{\lambda_{\Lambda^*},\lambda_p}(\phi_K,\theta_{\Lambda^*},0)^* R_{\Lambda_n^*}(m_{Kp}) \times D^1_{\lambda_\psi,\Delta\lambda_\mu}(\phi_\mu,\theta_\psi,0)^*, \quad (3)$$

where the x axis, in the coordinates describing the Λ_b^0 decay, is chosen to fix $\phi_{\Lambda^*} = 0$. The sum over n is due to many different Λ_n^* resonances contributing to the amplitude. Since the J/ψ decay is electromagnetic, the values of $\Delta\lambda_\mu \equiv \lambda_{\mu^+} - \lambda_{\mu^-}$ are restricted to ± 1.

There are four (six) independent complex $\mathcal{H}^{\Lambda_b^0\to\Lambda_n^*\psi}_{\lambda_{\Lambda^*},\lambda_\psi}$ couplings to fit for each Λ_n^* resonance for $J_{\Lambda_n^*} = \frac{1}{2}$ ($> \frac{1}{2}$). They can be reduced to only one (three) free $B_{L,S}$ coupling to fit if only the lowest (the lowest two) values of L are considered. The mass m_{Kp}, together with all decay angles entering Eq. (3), $\theta_{\Lambda_b^0}$, θ_{Λ^*}, ϕ_K, θ_ψ, and ϕ_μ (denoted collectively as Ω), constitute the six independent dimensions of the $\Lambda_b^0 \to J/\psi p K^-$ decay phase space.

Similarly, the matrix element for the P_c^+ decay chain is given by

$$\mathcal{M}^{P_c}_{\lambda_{\Lambda_b^0},\lambda_p^{P_c},\Delta\lambda_\mu^{P_c}} \equiv \sum_j \sum_{\lambda_{P_c}} \sum_{\lambda_\psi^{P_c}} \mathcal{H}^{\Lambda_b^0\to P_{cj}K}_{\lambda_{P_c},0} D^{1/2}_{\lambda_{\Lambda_b^0},\lambda_{P_c}}(\phi_{P_c},\theta^{P_c}_{\Lambda_b^0},0)^* \times \mathcal{H}^{P_{cj}\to\psi p}_{\lambda_\psi^{P_c},\lambda_p^{P_c}} D^{J_{P_{cj}}}_{\lambda_{P_c},\lambda_\psi^{P_c}-\lambda_p^{P_c}}(\phi_\psi,\theta_{P_c},0)^* R_{P_{cj}}(m_{\psi p}) \times D^1_{\lambda_\psi^{P_c},\Delta\lambda_\mu^{P_c}}(\phi^{P_c}_\mu,\theta^{P_c}_\psi,0)^*, \quad (4)$$

where the angles and helicity states carry the superscript or subscript P_c to distinguish them from those defined for the Λ^* decay chain. The sum over j allows for the possibility of contributions from more than one P_c^+ resonance. There are two (three) independent helicity couplings $\mathcal{H}^{P_{cj}\to\psi p}_{\lambda_\psi^{P_c},\lambda_p^{P_c}}$ for $J_{P_{cj}} = \frac{1}{2}$ ($> \frac{1}{2}$), and a ratio of the two $\mathcal{H}^{\Lambda_b^0\to P_{cj}K}_{\lambda_{P_c},0}$ couplings, to determine from the data.

The mass-dependent $R_{\Lambda_n^*}(m_{Kp})$ and $R_{P_{cj}}(m_{J/\psi p})$ terms are given by

$$R_X(m) = B'_{L^X_{\Lambda_b^0}}(p,p_0,d)\left(\frac{p}{M_{\Lambda_b^0}}\right)^{L^X_{\Lambda_b^0}} \times \mathrm{BW}(m|M_{0X},\Gamma_{0X}) B'_{L_X}(q,q_0,d)\left(\frac{q}{M_{0X}}\right)^{L_X}. \quad (5)$$

Here p is the $X = \Lambda^*$ or P_c^+ momentum in the Λ_b^0 rest frame, and q is the momentum of either decay product of X in the X rest frame. The symbols p_0 and q_0 denote values of these quantities at the resonance peak ($m = M_{0X}$). The orbital angular momentum between the decay products of Λ_b^0 is denoted as $L^X_{\Lambda_b^0}$. Similarly, L_X is the orbital angular momentum between the decay products of X. The orbital angular momentum barrier factors, $p^L B'_L(p,p_0,d)$, involve the Blatt-Weisskopf functions [29], and account for the difficulty in creating larger orbital angular momentum L, which depends on the momentum of the decay products p and on the size of the decaying particle, given by the d constant. We set $d = 3.0\ \mathrm{GeV}^{-1} \sim 0.6$ fm. The relativistic Breit-Wigner amplitude is given by

$$\mathrm{BW}(m|M_{0X},\Gamma_{0X}) = \frac{1}{{M_{0X}}^2 - m^2 - iM_{0X}\Gamma(m)}, \quad (6)$$

where

$$\Gamma(m) = \Gamma_{0X}\left(\frac{q}{q_0}\right)^{2L_X+1} \frac{M_{0X}}{m} B'_{L_X}(q,q_0,d)^2 \quad (7)$$

is the mass-dependent width of the resonance. For the $\Lambda(1405)$ resonance, which peaks below the K^-p threshold, we use a two-component Flatté-like parametrization [30]

(see the Supplemental Material [20]). The couplings for the allowed channels, $\Sigma\pi$ and Kp, are taken to be equal and to correspond to the nominal value of the width [12]. For all resonances we assume minimal values of $L^X_{\Lambda^0_b}$ and of L_X in $R_X(m)$. For nonresonant (NR) terms we set $\mathrm{BW}(m) = 1$ and $M_{0\mathrm{NR}}$ to the midrange mass.

Before the matrix elements for the two decay sequences can be added coherently, the proton and muon helicity states in the Λ^* decay chain must be expressed in the basis of helicities in the P_c^+ decay chain,

$$|\mathcal{M}|^2 = \sum_{\lambda_{\Lambda^0_b}} \sum_{\lambda_p} \sum_{\Delta\lambda_\mu} \left| \mathcal{M}^{\Lambda^*}_{\lambda_{\Lambda^0_b}, \lambda_p, \Delta\lambda_\mu} + e^{i\Delta\lambda_\mu \alpha_\mu} \sum_{\lambda_p^{P_c}} d^{1/2}_{\lambda_p^{P_c}, \lambda_p}(\theta_p) \mathcal{M}^{P_c}_{\lambda_{\Lambda^0_b}, \lambda_p^{P_c}, \Delta\lambda_\mu} \right|^2, \quad (8)$$

where θ_p is the polar angle in the p rest frame between the boost directions from the Λ^* and P_c^+ rest frames, and α_μ is the azimuthal angle correcting for the difference between the muon helicity states in the two decay chains. Note that $m_{\psi p}$, $\theta^{P_c}_{\Lambda b}$, ϕ_{P_c}, θ_{P_c}, ϕ_ψ, $\theta^{P_c}_\psi$, $\phi^{P_c}_\mu$, θ_p, and α_μ can all be derived from the values of m_{Kp} and Ω, and thus do not constitute independent dimensions in the Λ^0_b decay phase space. (A detailed prescription for calculation of all the angles entering the matrix element is given in the Supplemental Material [20].)

Strong interactions, which dominate Λ^0_b production at the LHC, conserve parity and cannot produce longitudinal Λ^0_b polarization [31]. Therefore, $\lambda_{\Lambda^0_b} = +1/2$ and $-1/2$ values are equally likely, which is reflected in Eq. (8). If we allow the Λ^0_b polarization to vary, the data are consistent with a polarization of zero. Interferences between various Λ^*_n and P^+_{cj} resonances vanish in the integrated rates unless the resonances belong to the same decay chain and have the same quantum numbers.

The matrix element given by Eq. (8) is a six-dimensional function of m_{Kp} and Ω and depends on the fit parameters, $\vec{\omega}$, which represent independent helicity or LS couplings, and masses and widths of resonances (or Flatté parameters), $\mathcal{M} = \mathcal{M}(m_{Kp}, \Omega|\vec{\omega})$. After accounting for the selection efficiency to obtain the signal probability density function (PDF), an unbinned maximum likelihood fit is used to determine the amplitudes. Since the efficiency does not depend on $\vec{\omega}$, it is needed only in the normalization integral, which is carried out numerically by summing $|\mathcal{M}(m_{Kp}, \Omega|\vec{\omega})|^2$ over the simulated events generated uniformly in phase space and passed through the selection. (More details are given in the Supplemental Material [20].)

We use two fit algorithms, which were independently coded and which differ in the approach used for background subtraction. In the first approach, which we refer to as cFit, the signal region is defined as $\pm 2\sigma$ around the Λ^0_b mass peak. The total PDF used in the fit to the candidates in the signal region, $\mathcal{P}(m_{Kp}, \Omega|\vec{\omega})$, includes a background component with normalization fixed to be 5.4% of the total. The background PDF is found to factorize into five two-dimensional functions of m_{Kp} and of each independent angle, which are estimated using sidebands extending from 5.0σ to 13.5σ on both sides of the peak.

In the complementary approach, called sFit, no explicit background parametrization is needed. The PDF consists of only the signal component, with the background subtracted using the sPlot technique [32] applied to the log-likelihood sum. All candidates shown in Fig. 4 are included in the sum with weights, W_i, dependent on $m_{J/\psi Kp}$. The weights are set according to the signal and the background probabilities determined by the fits to the $m_{J/\psi pK}$ distributions, similar to the fit displayed in Fig. 4, but performed in 32 different bins of the two-dimensional plane of $\cos\theta_{\Lambda^0_b}$ and $\cos\theta_{J/\psi}$ to account for correlations with the mass shapes of the signal and background components. This quasi-log-likelihood sum is scaled by a constant factor, $s_W \equiv \sum_i W_i / \sum_i {W_i}^2$, to account for the effect of the background subtraction on the statistical uncertainty. (More details on the cFit and sFit procedures are given in the Supplemental Material [20].)

In each approach, we minimize $-2\ln\mathcal{L}(\vec{\omega}) = -2 s_W \sum_i W_i \ln \mathcal{P}(m_{Kp_i}, \Omega_i|\vec{\omega})$, which gives the estimated values of the fit parameters, $\vec{\omega}_{\min}$, together with their covariance matrix ($W_i = 1$ in cFit). The difference of $-2\ln\mathcal{L}(\vec{\omega}_{\min})$ between different amplitude models, $\Delta(-2\ln\mathcal{L})$, allows their discrimination. For two models representing separate hypotheses, e.g., when discriminating between different J^P values assigned to a P_c^+ state, the assumption of a χ^2 distribution with 1 degree of freedom for $\Delta(-2\ln\mathcal{L})$ under the disfavored J^P hypothesis allows the calculation of a lower limit on the significance of its rejection, i.e., the p value [33]. Therefore, it is convenient to express $\Delta(-2\ln\mathcal{L})$ values as n^2_σ, where n_σ corresponds to the number of standard deviations in the normal distribution with the same p value. For nested hypotheses, e.g., when discriminating between models without and with P_c^+ states, n_σ overestimates the p value by a modest amount. Simulations are used to obtain better estimates of the significance of the P_c^+ states.

Since the isospin of both the Λ^0_b and the J/ψ particles are zero, we expect that the dominant contributions in the K^-p system are Λ^* states, which would be produced via a $\Delta I = 0$ process. It is also possible that Σ^* resonances contribute, but these would have $\Delta I = 1$. By analogy with kaon decays the $\Delta I = 0$ process should be dominant [34]. The list of Λ^* states considered is shown in Table I.

Our strategy is to first try to fit the data with a model that can describe the mass and angular distributions including only Λ^* resonances, allowing all possible known states and decay amplitudes. We call this the "extended" model. It has

TABLE I. The Λ^* resonances used in the different fits. Parameters are taken from the PDG [12]. We take $5/2^-$ for the J^P of the $\Lambda(2585)$. The number of LS couplings is also listed for both the reduced and extended models. To fix overall phase and magnitude conventions, which otherwise are arbitrary, we set $B_{0,\frac{1}{2}} = (1, 0)$ for $\Lambda(1520)$. A zero entry means the state is excluded from the fit.

State	J^P	M_0 (MeV)	Γ_0 (MeV)	Number Reduced	Number Extended
$\Lambda(1405)$	$1/2^-$	$1405.1^{+1.3}_{-1.0}$	50.5 ± 2.0	3	4
$\Lambda(1520)$	$3/2^-$	1519.5 ± 1.0	15.6 ± 1.0	5	6
$\Lambda(1600)$	$1/2^+$	1600	150	3	4
$\Lambda(1670)$	$1/2^-$	1670	35	3	4
$\Lambda(1690)$	$3/2^-$	1690	60	5	6
$\Lambda(1800)$	$1/2^-$	1800	300	4	4
$\Lambda(1810)$	$1/2^+$	1810	150	3	4
$\Lambda(1820)$	$5/2^+$	1820	80	1	6
$\Lambda(1830)$	$5/2^-$	1830	95	1	6
$\Lambda(1890)$	$3/2^+$	1890	100	3	6
$\Lambda(2100)$	$7/2^-$	2100	200	1	6
$\Lambda(2110)$	$5/2^+$	2110	200	1	6
$\Lambda(2350)$	$9/2^+$	2350	150	0	6
$\Lambda(2585)$	?	$\approx$2585	200	0	6

146 free parameters from the helicity couplings alone. The masses and widths of the Λ^* states are fixed to their PDG values, since allowing them to float prevents the fit from converging. Variations in these parameters are considered in the systematic uncertainties.

The cFit results without any P_c^+ component are shown in Fig. 6. While the m_{Kp} distribution is reasonably well fitted, the peaking structure in $m_{J/\psi p}$ is not reproduced. The same result is found using sFit. The speculative addition of Σ^* resonances to the states decaying to K^-p does not change this conclusion.

We will demonstrate that introducing two $P_c^+ \to J/\psi p$ resonances leads to a satisfactory description of the data. When determining parameters of the P_c^+ states, we use a more restrictive model of the K^-p states (hereafter referred to as the "reduced" model) that includes only the Λ^* resonances that are well motivated, and has fewer than half the number of free parameters. As the minimal $L^{\Lambda^*}_{\Lambda_b^0}$ for the spin $9/2$ $\Lambda(2350)$ equals $J_{\Lambda^*} - J_{\Lambda_b^0} - J_{J/\psi} = 3$, it is extremely unlikely that this state can be produced so close to the phase space limit. In fact $L = 3$ is the highest orbital angular momentum observed, with a very small rate, in decays of B mesons [35] with much larger phase space available ($Q = 2366$ MeV, while here $Q = 173$ MeV), and without additional suppression from the spin counting factors present in $\Lambda(2350)$ production (all three $\vec{J}_{\Lambda^*}$, $\vec{J}_{\Lambda_b^0}$ and $\vec{J}_{J/\psi}$ vectors have to line up in the same direction to produce the minimal $L^{\Lambda^*}_{\Lambda_b^0}$ value). Therefore, we eliminate it

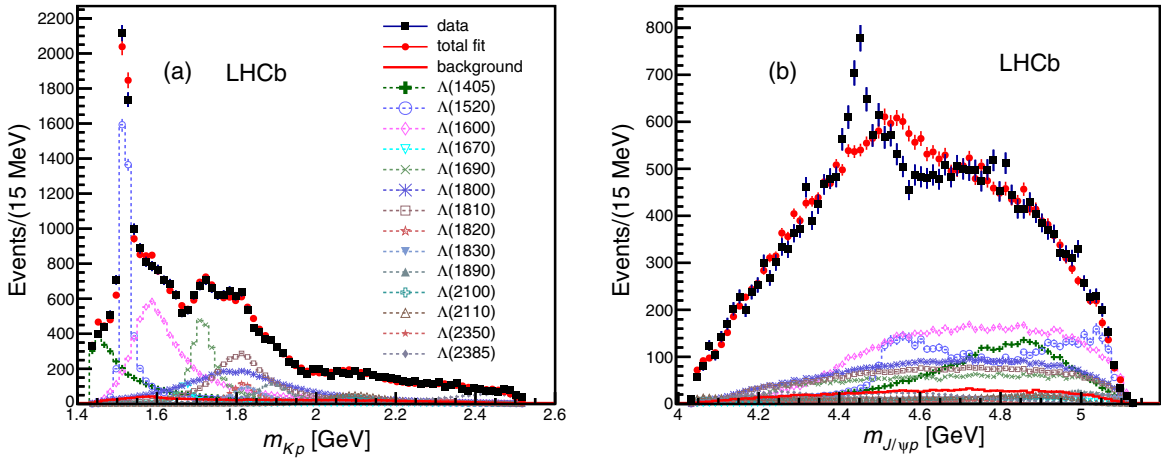

FIG. 6 (color online). Results for (a) m_{Kp} and (b) $m_{J/\psi p}$ for the extended Λ^* model fit without P_c^+ states. The data are shown as (black) squares with error bars, while the (red) circles show the results of the fit. The error bars on the points showing the fit results are due to simulation statistics.

from the reduced Λ^* model. We also eliminate the $\Lambda(2585)$ state, which peaks beyond the kinematic limit and has unknown spin. The other resonances are kept but high $L^{\Lambda^*}_{\Lambda^0_b}$ amplitudes are removed; only the lowest values are kept for the high mass resonances, with a smaller reduction for the lighter ones. The number of LS amplitudes used for each resonance is listed in Table I. With this model, we reduce the number of parameters needed to describe the Λ^* decays from 146 to 64. For the different combinations of P_c^+ resonances that we try, there are up to 20 additional free parameters. Using the extended model including one resonant P_c^+ improves the fit quality, but it is still unacceptable (see Supplemental Material [20]). We find acceptable fits with two P_c^+ states. We use the reduced Λ^* model for the central values of our results. The differences in fitted quantities with the extended model are included in the systematic uncertainties.

The best fit combination finds two P_c^+ states with J^P values of $3/2^-$ and $5/2^+$, for the lower and higher mass states, respectively. The $-2\ln\mathcal{L}$ values differ by only 1 unit between the best fit and the parity reversed combination $(3/2^+, 5/2^-)$. Other combinations are less likely, although the $(5/2^+, 3/2^-)$ pair changes $-2\ln\mathcal{L}$ by only 2.3^2 units and therefore cannot be ruled out. All combinations $1/2^\pm$ through $7/2^\pm$ were tested, and all others are disfavored by changes of more than 5^2 in the $-2\ln\mathcal{L}$ values. The cFit results for the $(3/2^-, 5/2^+)$ fit are shown in Fig. 3. Both distributions of m_{Kp} and $m_{J/\psi p}$ are reproduced. The lower mass $3/2^-$ state has mass 4380 ± 8 MeV and width 205 ± 18 MeV, while the $5/2^+$ state has a mass of 4449.8 ± 1.7 MeV and width 39 ± 5 MeV. These errors are statistical only; systematic uncertainties are discussed later. The mass resolution is approximately 2.5 MeV and does not affect the width determinations. The sFit approach gives comparable results. The angular distributions are reasonably well reproduced, as shown in Fig. 7, and the comparison with the data in m_{Kp} intervals is also satisfactory as can be seen in Fig. 8. Interference effects between

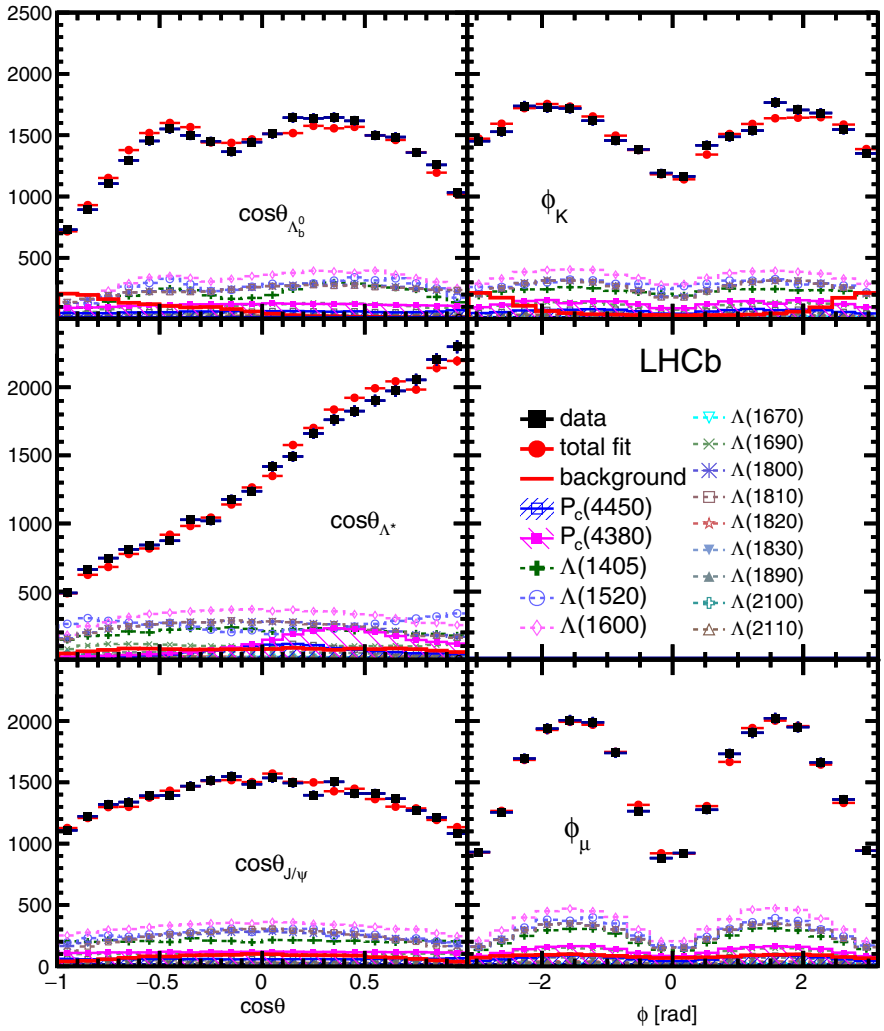

FIG. 7 (color online). Various decay angular distributions for the fit with two P_c^+ states. The data are shown as (black) squares, while the (red) circles show the results of the fit. Each fit component is also shown. The angles are defined in the text.

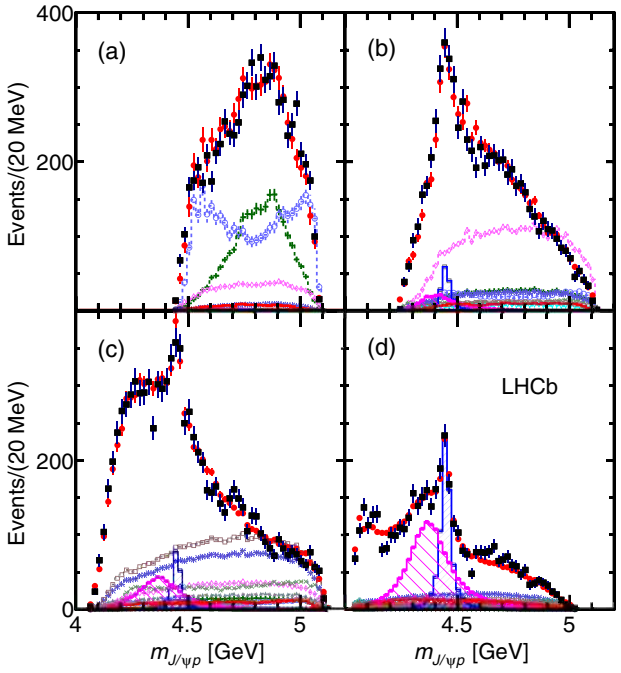

FIG. 8 (color online). $m_{J/\psi p}$ in various intervals of m_{Kp} for the fit with two P_c^+ states: (a) $m_{Kp} < 1.55$ GeV, (b) $1.55 < m_{Kp} < 1.70$ GeV, (c) $1.70 < m_{Kp} < 2.00$ GeV, and (d) $m_{Kp} > 2.00$ GeV. The data are shown as (black) squares with error bars, while the (red) circles show the results of the fit. The blue and purple histograms show the two P_c^+ states. See Fig. 7 for the legend.

the two P_c^+ states are particularly evident in Fig. 8(d), where there is a large destructive contribution (not explicitly shown in the figure) to the total rate. (A fit fraction comparison between cFit and sFit is given in the Supplemental Material [20].) The addition of further P_c^+ states does not significantly improve the fit.

Adding a single $5/2^+ P_c^+$ state to the fit with only Λ^* states reduces $-2\ln\mathcal{L}$ by 14.7^2 using the extended model and adding a second lower mass $3/2^-$ P_c^+ state results in a further reduction of 11.6^2. The combined reduction of $-2\ln\mathcal{L}$ by the two states taken together is 18.7^2. Since taking $\sqrt{\Delta 2\ln\mathcal{L}}$ overestimates significances, we perform simulations to obtain more accurate evaluations. We generate pseudoexperiments using the null hypotheses having amplitude parameters determined by the fits to the data with no or one P_c^+ state. We fit each pseudoexperiment with the null hypothesis and with P_c^+ states added to the model. The $-2\ln\mathcal{L}$ distributions obtained from many pseudoexperiments are consistent with χ^2 distributions with the number of degrees of freedom approximately equal to twice the number of extra parameters in the fit. Comparing these distributions with the $\Delta 2\ln\mathcal{L}$ values from the fits to the data, p values can be calculated. These studies show reduction of the significances relative to $\sqrt{\Delta 2\ln\mathcal{L}}$ by about 20%, giving overall significances of 9σ and 12σ, for the lower and higher mass P_c^+ states, respectively. The combined significance of two P_c^+ states is 15σ. Use of the extended model to evaluate the significance includes the effect of systematic uncertainties due to the possible presence of additional Λ^* states or higher L amplitudes.

Systematic uncertainties are evaluated for the masses, widths, and fit fractions of the P_c^+ states, and for the fit fractions of the two lightest and most significant Λ^* states. Additional sources of modeling uncertainty that we have not considered may affect the fit fractions of the heavier Λ^* states. The sources of systematic uncertainties are listed in Table II. They include differences between the results of the extended versus reduced model, varying the Λ^* masses and widths, uncertainties in the identification requirements for the proton and restricting its momentum, inclusion of a nonresonant amplitude in the fit, use of separate higher and lower Λ_b^0 mass sidebands, alternate J^P fits, varying the Blatt-Weisskopf barrier factor d between 1.5 and 4.5 GeV^{-1}, changing the angular momentum L used in Eq. (5) by one or two units, and accounting for potential mismodeling of the efficiencies. For the $\Lambda(1405)$ fit fraction we also added an uncertainty for the Flatté couplings, determined by both halving and doubling their ratio, and taking the maximum deviation as the uncertainty.

The stability of the results is cross-checked by comparing the data recorded in 2011 (2012), with the LHCb dipole magnet polarity in up (down) configurations, $\Lambda_b^0(\bar{\Lambda}_b^0)$ decays, and Λ_b^0 produced with low (high) values of p_T. Extended model fits without including P_c^+ states were tried with the addition of two high mass Λ^* resonances of freely varied mass and width, or four nonresonant components up to spin $3/2$; these do not explain the data. The fitters were tested on simulated pseudoexperiments and no biases were found. In addition, selection requirements are varied, and the vetoes of $\bar{B}_s^0$ and $\bar{B}^0$ are removed and explicit models of those backgrounds added to the fit; all give consistent results.

Further evidence for the resonant character of the higher mass, narrower P_c^+ state is obtained by viewing the evolution of the complex amplitude in the Argand diagram [12]. In the amplitude fits discussed above, the $P_c(4450)^+$ is represented by a Breit-Wigner amplitude, where the magnitude and phase vary with $m_{J/\psi p}$ according to an approximately circular trajectory in the ($\text{Re}A^{P_c}$, $\text{Im}A^{P_c}$) plane, where A^{P_c} is the $m_{J/\psi p}$ dependent part of the $P_c(4450)^+$ amplitude. We perform an additional fit to the data using the reduced Λ^* model, in which we represent the $P_c(4450)^+$ amplitude as the combination of independent complex amplitudes at six equidistant points in the range $\pm\Gamma_0 = 39$ MeV around $M_0 = 4449.8$ MeV as determined in the default fit. Real and imaginary parts of the amplitude are interpolated in the mass interval between the fitted points. The resulting Argand diagram, shown in Fig. 9(a), is consistent with a rapid counterclockwise change of the $P_c(4450)^+$ phase when its magnitude reaches

TABLE II. Summary of systematic uncertainties on P_c^+ masses, widths, and fit fractions, and Λ^* fit fractions. A fit fraction is the ratio of the phase space integrals of the matrix element squared for a single resonance and for the total amplitude. The terms "low" and "high" correspond to the lower and higher mass P_c^+ states. The sFit–cFit difference is listed as a cross-check and not included as an uncertainty.

Source	M_0 (MeV)		Γ_0 (MeV)		Fit Fractions (%)			
	Low	High	Low	High	Low	High	$\Lambda(1405)$	$\Lambda(1520)$
Extended versus reduced	21	0.2	54	10	3.14	0.32	1.37	0.15
Λ^* masses and widths	7	0.7	20	4	0.58	0.37	2.49	2.45
Proton ID	2	0.3	1	2	0.27	0.14	0.20	0.05
$10 < p_p < 100$ GeV	0	1.2	1	1	0.09	0.03	0.31	0.01
Nonresonant	3	0.3	34	2	2.35	0.13	3.28	0.39
Separate sidebands	0	0	5	0	0.24	0.14	0.02	0.03
J^P $(3/2^+, 5/2^-)$ or $(5/2^+, 3/2^-)$	10	1.2	34	10	0.76	0.44		
$d = 1.5$–4.5GeV^{-1}	9	0.6	19	3	0.29	0.42	0.36	1.91
$L^{P_c}_{\Lambda_b^0}$ $\Lambda_b^0 \to P_c^+$ (low or high) K^-	6	0.7	4	8	0.37	0.16		
L_{P_c} P_c^+(low or high) $\to J/\psi p$	4	0.4	31	7	0.63	0.37		
$L^{\Lambda_n^*}_{\Lambda_b^0}$ $\Lambda_b^0 \to J/\psi\Lambda^*$	11	0.3	20	2	0.81	0.53	3.34	2.31
Efficiencies	1	0.4	4	0	0.13	0.02	0.26	0.23
Change $\Lambda(1405)$ coupling	0	0	0	0	0	0	1.90	0
Overall	29	2.5	86	19	4.21	1.05	5.82	3.89
sFit/cFit cross-check	5	1.0	11	3	0.46	0.01	0.45	0.13

the maximum, a behavior characteristic of a resonance. A similar study for the wider state is shown in Fig. 9(b); although the fit does show a large phase change, the amplitude values are sensitive to the details of the Λ^* model and so this latter study is not conclusive.

Different binding mechanisms of pentaquark states are possible. Tight binding was envisioned originally [3,4,36]. A possible explanation is heavy-light diquarks [37]. Examples of other mechanisms include a diquark-diquark-antiquark model [38,39], a diquark-triquark model [40], and a coupled channel model [41]. Weakly bound "molecules" of a baryon plus a meson have been also discussed [42].

Models involving thresholds or "cusps" have been invoked to explain some exotic meson candidates via nonresonant scattering mechanisms [43–45]. There are certain obvious difficulties with the use of this approach to explain our results. The closest threshold to the high

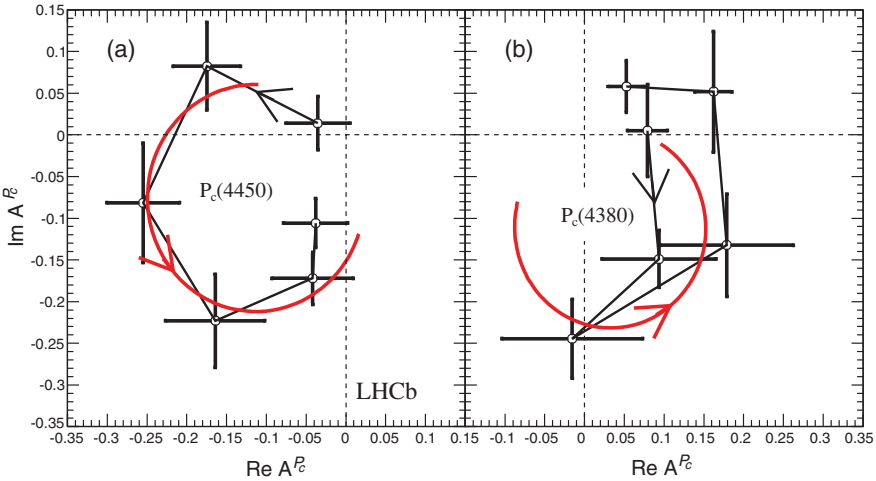

FIG. 9 (color online). Fitted values of the real and imaginary parts of the amplitudes for the baseline $(3/2^-, 5/2^+)$ fit for (a) the $P_c(4450)^+$ state and (b) the $P_c(4380)^+$ state, each divided into six $m_{J/\psi p}$ bins of equal width between $-\Gamma_0$ and $+\Gamma_0$ shown in the Argand diagrams as connected points with error bars ($m_{J/\psi p}$ increases counterclockwise). The solid (red) curves are the predictions from the Breit-Wigner formula for the same mass ranges with M_0 (Γ_0) of 4450 (39) MeV and 4380 (205) MeV, respectively, with the phases and magnitudes at the resonance masses set to the average values between the two points around M_0. The phase convention sets $B_{0,\frac{1}{2}} = (1, 0)$ for $\Lambda(1520)$. Systematic uncertainties are not included.

mass state is at 4457.1 ± 0.3 MeV resulting from a $\Lambda_c(2595)^+\bar{D}^0$ combination, which is somewhat higher than the peak mass value and would produce a structure with quantum numbers $J^P = 1/2^+$ which are disfavored by our data. There is no threshold close to the lower mass state.

In conclusion, we have presented a full amplitude fit to the $\Lambda_b^0 \to J/\psi K^- p$ decay. We observe significant Λ^* production recoiling against the J/ψ with the lowest mass contributions, the $\Lambda(1405)$ and $\Lambda(1520)$ states having fit fractions of $(15 \pm 1 \pm 6)\%$ and $(19 \pm 1 \pm 4)\%$, respectively. The data cannot be satisfactorily described without including two Breit-Wigner shaped resonances in the $J/\psi p$ invariant mass distribution. The significances of the lower mass and higher mass states are 9 and 12 standard deviations, respectively. These structures cannot be accounted for by reflections from $J/\psi\Lambda^*$ resonances or other known sources. Interpreted as resonant states they must have minimal quark content of $c\bar{c}uud$, and would therefore be called charmonium-pentaquark states. The lighter state $P_c(4380)^+$ has a mass of $4380 \pm 8 \pm 29$ MeV and a width of $205 \pm 18 \pm 86$ MeV, while the heavier state $P_c(4450)^+$ has a mass of $4449.8 \pm 1.7 \pm 2.5$ MeV and a width of $39 \pm 5 \pm 19$ MeV. A model-independent representation of the $P_c(4450)^+$ contribution in the fit shows a phase change in amplitude consistent with that of a resonance. The parities of the two states are opposite with the preferred spins being $3/2$ for one state and $5/2$ for the other. The higher mass state has a fit fraction of $(4.1 \pm 0.5 \pm 1.1)\%$, and the lower mass state of $(8.4 \pm 0.7 \pm 4.2)\%$, of the total $\Lambda_b^0 \to J/\psi K^- p$ sample.

We express our gratitude to our colleagues in the CERN accelerator departments for the excellent performance of the LHC. We thank the technical and administrative staff at the LHCb institutes. We acknowledge support from CERN and from the national agencies: CAPES, CNPq, FAPERJ, and FINEP (Brazil); NSFC (China); CNRS/IN2P3 (France); BMBF, DFG, HGF, and MPG (Germany); INFN (Italy); FOM and NWO (The Netherlands); MNiSW and NCN (Poland); MEN/IFA (Romania); MinES and FANO (Russia); MinECo (Spain); SNSF and SER (Switzerland); NASU (Ukraine); STFC (U.K.); and NSF (U.S.). The Tier1 computing centers are supported by IN2P3 (France), KIT and BMBF (Germany), INFN (Italy), NWO and SURF (The Netherlands), PIC (Spain), and GridPP (United Kingdom). We are indebted to the communities behind the multiple open source software packages on which we depend. We are also thankful for the computing resources and the access to software research and development tools provided by Yandex LLC (Russia). Individual groups or members have received support from EPLANET, Marie Skłodowska-Curie Actions, and ERC (European Union); Conseil général de Haute-Savoie, Labex ENIGMASS, and OCEVU, Région Auvergne (France); RFBR (Russia); XuntaGal and GENCAT (Spain); and the Royal Society and Royal Commission for the Exhibition of 1851 (United Kingdom).

[1] M. Gell-Mann, A schematic model of baryons and mesons, Phys. Lett. **8**, 214 (1964).
[2] G. Zweig, Report No. CERN-TH-401.
[3] R. L. Jaffe, Multiquark hadrons. I. Phenomenology of $Q^2\bar{Q}^2$ mesons, Phys. Rev. D **15**, 267 (1977).
[4] D. Strottman, Multi-quark baryons and the MIT bag model, Phys. Rev. D **20**, 748 (1979); H. Hogaasen and P. Sorba, The systematics of possibly narrow quark states with baryon number one, Nucl. Phys. **B145**, 119 (1978).
[5] H. J. Lipkin, New possibilities for exotic hadrons: Anticharmed strange baryons, Phys. Lett. B **195**, 484 (1987).
[6] K. H. Hicks, On the conundrum of the pentaquark, Eur. Phys. J. H **37**, 1 (2012).
[7] S. K. Choi *et al.* (Belle Collaboration), Observation of a Resonancelike Structure in the $\pi^\pm\psi'$ Mass Distribution in Exclusive $B \to K\pi^\pm\psi'$ Decays, Phys. Rev. Lett. **100**, 142001 (2008).
[8] K. Chilikin *et al.* (Belle Collaboration), Experimental constraints on the spin and parity of the $Z(4430)^+$, Phys. Rev. D **88**, 074026 (2013).
[9] R. Aaij *et al.* (LHCb Collaboration), Observation of the Resonant Character of the $Z(4430)^-$ State, Phys. Rev. Lett. **112**, 222002 (2014).
[10] X.-Q. Li and X. Liu, A possible global group structure for exotic states, Eur. Phys. J. C **74**, 3198 (2014).
[11] R. Aaij *et al.* (LHCb Collaboration), Precision measurement of the ratio of the Λ_b^0 to $\bar{B}^0$ lifetimes, Phys. Lett. B **734**, 122 (2014); Precision Measurement of the Λ_b^0 Baryon Lifetime, Phys. Rev. Lett. **111**, 102003 (2013).
[12] K. A. Olive *et al.* (Particle Data Group), Review of particle physics, Chin. Phys. C **38**, 090001 (2014).
[13] A. A. Alves Jr. *et al.* (LHCb Collaboration), The LHCb detector at the LHC, JINST **3**, S08005 (2008).
[14] R. Aaij *et al.*, Performance of the LHCb vertex locator, JINST **9**, P09007 (2014).
[15] R. Arink *et al.*, Performance of the LHCb outer tracker, JINST **9**, P01002 (2014).
[16] M. Adinolfi *et al.*, Performance of the LHCb RICH detector at the LHC, Eur. Phys. J. C **73**, 2431 (2013).
[17] A. A. Alves Jr. *et al.*, Performance of the LHCb muon system, JINST **8**, P02022 (2013).
[18] R. Aaij *et al.* (LHCb Collaboration), First observation of $B_s^0 \to J/\psi f_0(980)$ decays, Phys. Lett. B **698**, 115 (2011).
[19] L. Breiman, J. H. Friedman, R. A. Olshen, and C. J. Stone, *Classification and Regression Trees* (Wadsworth International Group, Belmont, CA, 1984); A. Hoecker *et al.*, TMVA: Toolkit for multivariate data analysis, *Proc. Sci.*, ACAT (2007) 040 [arXiv:physics/0703039].
[20] See Supplemental Material at http://link.aps.org/supplemental/10.1103/PhysRevLett.115.072001 for additional information on the variables used in the BDTG, additional fit results, the fit fraction comparison between cFit and sFit, and details of the decay amplitude and fitting techniques.

[21] T. Sjöstrand, S. Mrenna, and P. Skands, PYTHIA 6.4 physics and manual, J. High Energy Phys. 05 (2006) 026; T. Sjöstrand, S. Mrenna, and P. Skands, A brief introduction to PYTHIA 8.1, Comput. Phys. Commun. **178**, 852 (2008).

[22] I. Belyaev *et al.*, Handling of the generation of primary events in Gauss, the LHCb simulation framework, J. Phys. Conf. Ser. **331**, 032047 (2011).

[23] S. Agostinelli *et al.* (Geant4 Collaboration), Geant4: A simulation toolkit, Nucl. Instrum. Methods Phys. Res., Sect. A **506**, 250 (2003); J. Allison *et al.* (Geant4 Collaboration), Geant4 developments and applications, IEEE Trans. Nucl. Sci. **53**, 270 (2006).

[24] M. Clemencic, G. Corti, S. Easo, C. R. Jones, S. Miglioranzi, M. Pappagallo, and P. Robbe, The LHCb simulation application, Gauss: Design, evolution, and experience, J. Phys. Conf. Ser. **331**, 032023 (2011).

[25] D. Martínez Santos and F. Dupertuis, Mass distributions marginalized over per-event errors, Nucl. Instrum. Methods Phys. Res., Sect. A **764**, 150 (2014).

[26] W. D. Hulsbergen, Decay chain fitting with a Kalman filter, Nucl. Instrum. Methods Phys. Res., Sect. A **552**, 566 (2005).

[27] R. H. Dalitz, On the analysis of τ-meson data and the nature of the τ meson, Philos. Mag. Ser. 5 **44**, 1068 (1953).

[28] S. U. Chung, Report No. CERN-71-08; J. D. Richman, Report No. CALT-68-1148; M. Jacob and G. C. Wick, On the general theory of collisions for particles with spin, Ann. Phys. (N.Y.) **7**, 404 (1959).

[29] F. Von Hippel and C. Quigg, Centrifugal-barrier effects in resonance partial decay widths, shapes, and production amplitudes, Phys. Rev. D **5**, 624 (1972).

[30] S. M. Flatté, Coupled-channel analysis of the $\pi\eta$ and $K\bar{K}$ systems near $K\bar{K}$ threshold, Phys. Lett. **63B**, 224 (1976).

[31] J. Soffer and N. A. Tornqvist, Origin of the Polarization for Inclusive Λ Production in pp Collisions, Phys. Rev. Lett. **68**, 907 (1992).

[32] M. Pivk and F. R. Le Diberder, sPlot: A statistical tool to unfold data distributions, Nucl. Instrum. Methods Phys. Res., Sect. A **555**, 356 (2005).

[33] F. James, *Statistical Methods in Experimental Physics* (World Scientific Publishing, Singapore, 2006).

[34] J. F. Donoghue, E. Golowich, W. A. Ponce, and B. R. Holstein, Analysis of $\Delta S = 1$ nonleptonic weak decays and the $\Delta I = \frac{1}{2}$ rule, Phys. Rev. D **21**, 186 (1980).

[35] R. Aaij *et al.* (LHCb Collaboration), Observation of Overlapping Spin-1 and Spin-3 $\bar{D}^0 K^-$ Resonances at Mass 2.86 GeV/c^2, Phys. Rev. Lett. **113**, 162001 (2014); Dalitz plot analysis of $B_s^0 \to \bar{D}^0 K^- \pi^+$ decays, Phys. Rev. D **90**, 072003 (2014).

[36] G. C. Rossi and G. Veneziano, A possible description of baryon dynamics in dual and gauge theories, Nucl. Phys. **B123**, 507 (1977).

[37] L. Maiani, F. Piccinini, A. D. Polosa, and V. Riquer, Diquark-antidiquarks with hidden or open charm and the nature of $X(3872)$, Phys. Rev. D **71**, 014028 (2005).

[38] R. Jaffe and F. Wilczek, Diquarks and Exotic Spectroscopy, Phys. Rev. Lett. **91**, 232003 (2003).

[39] A. Chandra, A. Bhattacharya, and B. Chakrabarti, Heavy pentaquarks and doubly heavy baryons in quasiparticle approach, Mod. Phys. Lett. A **27**, 1250006 (2012).

[40] M. Karliner and H. J. Lipkin, A diquark-triquark model for the KN pentaquark, Phys. Lett. B **575**, 249 (2003).

[41] J.-J. Wu, R. Molina, E. Oset, and B. S. Zou, Prediction of Narrow N^* and Λ^* Resonances with Hidden Charm Above 4 GeV, Phys. Rev. Lett. **105**, 232001 (2010).

[42] M. B. Voloshin and L. B. Okun, Hadron molecules and charmonium atom, JETP Lett. **23**, 333 (1976); A. De Rujula, H. Georgi, and S. L. Glashow, Molecular Charmonium: A New Spectroscopy?, Phys. Rev. Lett. **38**, 317 (1977); N. A. Törnqvist, Possible Large Deuteronlike Meson-Meson States Bound by Pions, Phys. Rev. Lett. **67**, 556 (1991); N. A. Törnqvist, From the deuteron to deusons, an analysis of deuteron-like meson-meson bound states, Z. Phys. C **61**, 525 (1994); Z.-C. Yang, Z.-F. Sun, J. He, X. Liu, and S.-L. Zhu, The possible hidden-charm molecular baryons composed of anti-charmed meson and charmed baryon, Chin. Phys. C **36**, 6 (2012); W. L. Wang, F. Huang, Z. Y. Zhang, and B. S. Zou, $\Sigma_c \bar{D}$ and $\Lambda_c \bar{D}$ states in a chiral quark model, Phys. Rev. C **84**, 015203 (2011); M. Karliner and J. L. Rosner, New exotic meson and baryon resonances from doubly-heavy hadronic molecules, arXiv: 1506.06386.

[43] E. S. Swanson, Cusps and exotic charmonia, arXiv: 1504.07952.

[44] E. S. Swanson, Z_b and Z_c exotic states as coupled channel cusps, Phys. Rev. D **91**, 034009 (2015).

[45] D. V. Bugg, An explanation of Belle states $Z_b(10610)$ and $Z_b(10650)$, Europhys. Lett. **96**, 11002 (2011).

R. Aaij,[38] B. Adeva,[37] M. Adinolfi,[46] A. Affolder,[52] Z. Ajaltouni,[5] S. Akar,[6] J. Albrecht,[9] F. Alessio,[38] M. Alexander,[51] S. Ali,[41] G. Alkhazov,[30] P. Alvarez Cartelle,[53] A. A. Alves Jr.,[57] S. Amato,[2] S. Amerio,[22] Y. Amhis,[7] L. An,[3] L. Anderlini,[17] J. Anderson,[40] G. Andreassi,[39] M. Andreotti,[16,f] J. E. Andrews,[58] R. B. Appleby,[54] O. Aquines Gutierrez,[10] F. Archilli,[38] P. d'Argent,[11] A. Artamonov,[35] M. Artuso,[59] E. Aslanides,[6] G. Auriemma,[25,m] M. Baalouch,[5] S. Bachmann,[11] J. J. Back,[48] A. Badalov,[36] C. Baesso,[60] W. Baldini,[16,38] R. J. Barlow,[54] C. Barschel,[38] S. Barsuk,[7] W. Barter,[38] V. Batozskaya,[28] V. Battista,[39] A. Bay,[39] L. Beaucourt,[4] J. Beddow,[51] F. Bedeschi,[23] I. Bediaga,[1] L. J. Bel,[41] V. Bellee,[39] N. Belloli,[20] I. Belyaev,[31] E. Ben-Haim,[8] G. Bencivenni,[18] S. Benson,[38] J. Benton,[46] A. Berezhnoy,[32] R. Bernet,[40] A. Bertolin,[22] M.-O. Bettler,[38] M. van Beuzekom,[41] A. Bien,[11] S. Bifani,[45] P. Billoir,[8] T. Bird,[54] A. Birnkraut,[9] A. Bizzeti,[17,h] T. Blake,[48] F. Blanc,[39] J. Blouw,[10] S. Blusk,[59] V. Bocci,[25] A. Bondar,[34] N. Bondar,[30,38] W. Bonivento,[15] S. Borghi,[54] M. Borsato,[7]

T. J. V. Bowcock,[52] E. Bowen,[40] C. Bozzi,[16] S. Braun,[11] M. Britsch,[10] T. Britton,[59] J. Brodzicka,[54] N. H. Brook,[46] A. Bursche,[40] J. Buytaert,[38] S. Cadeddu,[15] R. Calabrese,[16,f] M. Calvi,[20,j] M. Calvo Gomez,[36,o] P. Campana,[18] D. Campora Perez,[38] L. Capriotti,[54] A. Carbone,[14,d] G. Carboni,[24,k] R. Cardinale,[19,i] A. Cardini,[15] P. Carniti,[20] L. Carson,[50] K. Carvalho Akiba,[2,38] G. Casse,[52] L. Cassina,[20,j] L. Castillo Garcia,[38] M. Cattaneo,[38] Ch. Cauet,[9] G. Cavallero,[19] R. Cenci,[23,s] M. Charles,[8] Ph. Charpentier,[38] M. Chefdeville,[4] S. Chen,[54] S.-F. Cheung,[55] N. Chiapolini,[40] M. Chrzaszcz,[40] X. Cid Vidal,[38] G. Ciezarek,[41] P. E. L. Clarke,[50] M. Clemencic,[38] H. V. Cliff,[47] J. Closier,[38] V. Coco,[38] J. Cogan,[6] E. Cogneras,[5] V. Cogoni,[15,e] L. Cojocariu,[29] G. Collazuol,[22] P. Collins,[38] A. Comerma-Montells,[11] A. Contu,[15,38] A. Cook,[46] M. Coombes,[46] S. Coquereau,[8] G. Corti,[38] M. Corvo,[16,f] B. Couturier,[38] G. A. Cowan,[50] D. C. Craik,[48] A. Crocombe,[48] M. Cruz Torres,[60] S. Cunliffe,[53] R. Currie,[53] C. D'Ambrosio,[38] E. Dall'Occo,[41] J. Dalseno,[46] P. N. Y. David,[41] A. Davis,[57] K. De Bruyn,[41] S. De Capua,[54] M. De Cian,[11] J. M. De Miranda,[1] L. De Paula,[2] P. De Simone,[18] C.-T. Dean,[51] D. Decamp,[4] M. Deckenhoff,[9] L. Del Buono,[8] N. Déléage,[4] M. Demmer,[9] D. Derkach,[55] O. Deschamps,[5] F. Dettori,[38] B. Dey,[21] A. Di Canto,[38] F. Di Ruscio,[24] H. Dijkstra,[38] S. Donleavy,[52] F. Dordei,[11] M. Dorigo,[39] A. Dosil Suárez,[37] D. Dossett,[48] A. Dovbnya,[43] K. Dreimanis,[52] L. Dufour,[41] G. Dujany,[54] F. Dupertuis,[39] P. Durante,[38] R. Dzhelyadin,[35] A. Dziurda,[26] A. Dzyuba,[30] S. Easo,[49,38] U. Egede,[53] V. Egorychev,[31] S. Eidelman,[34] S. Eisenhardt,[50] U. Eitschberger,[9] R. Ekelhof,[9] L. Eklund,[51] I. El Rifai,[5] Ch. Elsasser,[40] S. Ely,[59] S. Esen,[11] H. M. Evans,[47] T. Evans,[55] A. Falabella,[14] C. Färber,[38] N. Farley,[45] S. Farry,[52] R. Fay,[52] D. Ferguson,[50] V. Fernandez Albor,[37] F. Ferrari,[14] F. Ferreira Rodrigues,[1] M. Ferro-Luzzi,[38] S. Filippov,[33] M. Fiore,[16,38,f] M. Fiorini,[16,f] M. Firlej,[27] C. Fitzpatrick,[39] T. Fiutowski,[27] K. Fohl,[38] P. Fol,[53] M. Fontana,[15] F. Fontanelli,[19,i] R. Forty,[38] O. Francisco,[2] M. Frank,[38] C. Frei,[38] M. Frosini,[17] J. Fu,[21] E. Furfaro,[24,k] A. Gallas Torreira,[37] D. Galli,[14,d] S. Gallorini,[22,38] S. Gambetta,[50] M. Gandelman,[2] P. Gandini,[55] Y. Gao,[3] J. García Pardiñas,[37] J. Garra Tico,[47] L. Garrido,[36] D. Gascon,[36] C. Gaspar,[38] R. Gauld,[55] L. Gavardi,[9] G. Gazzoni,[5] A. Geraci,[21,u] D. Gerick,[11] E. Gersabeck,[11] M. Gersabeck,[54] T. Gershon,[48] Ph. Ghez,[4] A. Gianelle,[22] S. Gianì,[39] V. Gibson,[47] O. G. Girard,[39] L. Giubega,[29] V. V. Gligorov,[38] C. Göbel,[60] D. Golubkov,[31] A. Golutvin,[53,31,38] A. Gomes,[1,a] C. Gotti,[20,j] M. Grabalosa Gándara,[5] R. Graciani Diaz,[36] L. A. Granado Cardoso,[38] E. Graugés,[36] E. Graverini,[40] G. Graziani,[17] A. Grecu,[29] E. Greening,[55] S. Gregson,[47] P. Griffith,[45] L. Grillo,[11] O. Grünberg,[63] B. Gui,[59] E. Gushchin,[33] Yu. Guz,[35,38] T. Gys,[38] T. Hadavizadeh,[55] C. Hadjivasiliou,[59] G. Haefeli,[39] C. Haen,[38] S. C. Haines,[47] S. Hall,[53] B. Hamilton,[58] X. Han,[11] S. Hansmann-Menzemer,[11] N. Harnew,[55] S. T. Harnew,[46] J. Harrison,[54] J. He,[38] T. Head,[39] V. Heijne,[41] K. Hennessy,[52] P. Henrard,[5] L. Henry,[8] J. A. Hernando Morata,[37] E. van Herwijnen,[38] M. Heß,[63] A. Hicheur,[2] D. Hill,[55] M. Hoballah,[5] C. Hombach,[54] W. Hulsbergen,[41] T. Humair,[53] N. Hussain,[55] D. Hutchcroft,[52] D. Hynds,[51] M. Idzik,[27] P. Ilten,[56] R. Jacobsson,[38] A. Jaeger,[11] J. Jalocha,[55] E. Jans,[41] A. Jawahery,[58] F. Jing,[3] M. John,[55] D. Johnson,[38] C. R. Jones,[47] C. Joram,[38] B. Jost,[38] N. Jurik,[59] S. Kandybei,[43] W. Kanso,[6] M. Karacson,[38] T. M. Karbach,[38,†] S. Karodia,[51] M. Kecke,[11] M. Kelsey,[59] I. R. Kenyon,[45] M. Kenzie,[38] T. Ketel,[42] B. Khanji,[20,38,j] C. Khurewathanakul,[39] S. Klaver,[54] K. Klimaszewski,[28] O. Kochebina,[7] M. Kolpin,[11] I. Komarov,[39] R. F. Koopman,[42] P. Koppenburg,[41,38] M. Kozeiha,[5] L. Kravchuk,[33] K. Kreplin,[11] M. Kreps,[48] G. Krocker,[11] P. Krokovny,[34] F. Kruse,[9] W. Krzemien,[28] W. Kucewicz,[26,n] M. Kucharczyk,[26] V. Kudryavtsev,[34] A. K. Kuonen,[39] K. Kurek,[28] T. Kvaratskheliya,[31] D. Lacarrere,[38] G. Lafferty,[54] A. Lai,[15] D. Lambert,[50] G. Lanfranchi,[18] C. Langenbruch,[48] B. Langhans,[38] T. Latham,[48] C. Lazzeroni,[45] R. Le Gac,[6] J. van Leerdam,[41] J.-P. Lees,[4] R. Lefèvre,[5] A. Leflat,[32,38] J. Lefrançois,[7] O. Leroy,[6] T. Lesiak,[26] B. Leverington,[11] Y. Li,[7] T. Likhomanenko,[65,64] M. Liles,[52] R. Lindner,[38] C. Linn,[38] F. Lionetto,[40] B. Liu,[15] X. Liu,[3] D. Loh,[48] I. Longstaff,[51] J. H. Lopes,[2] D. Lucchesi,[22,q] M. Lucio Martinez,[37] H. Luo,[50] A. Lupato,[22] E. Luppi,[16,f] O. Lupton,[55] N. Lusardi,[21] A. Lusiani,[23] F. Machefert,[7] F. Maciuc,[29] O. Maev,[30] K. Maguire,[54] S. Malde,[55] A. Malinin,[64] G. Manca,[7] G. Mancinelli,[6] P. Manning,[59] A. Mapelli,[38] J. Maratas,[5] J. F. Marchand,[4] U. Marconi,[14] C. Marin Benito,[36] P. Marino,[23,38,s] J. Marks,[11] G. Martellotti,[25] M. Martin,[6] M. Martinelli,[39] D. Martinez Santos,[37] F. Martinez Vidal,[66] D. Martins Tostes,[2] A. Massafferri,[1] R. Matev,[38] A. Mathad,[48] Z. Mathe,[38] C. Matteuzzi,[20] A. Mauri,[40] B. Maurin,[39] A. Mazurov,[45] M. McCann,[53] J. McCarthy,[45] A. McNab,[54] R. McNulty,[12] B. Meadows,[57] F. Meier,[9] M. Meissner,[11] D. Melnychuk,[28] M. Merk,[41] D. A. Milanes,[62] M.-N. Minard,[4] D. S. Mitzel,[11] J. Molina Rodriguez,[60] I. A. Monroy,[62] S. Monteil,[5] M. Morandin,[22] P. Morawski,[27] A. Mordà,[6] M. J. Morello,[23,s] J. Moron,[27] A. B. Morris,[50] R. Mountain,[59] F. Muheim,[50] J. Müller,[9] K. Müller,[40] V. Müller,[9] M. Mussini,[14] B. Muster,[39] P. Naik,[46] T. Nakada,[39] R. Nandakumar,[49] A. Nandi,[55] I. Nasteva,[2] M. Needham,[50] N. Neri,[21] S. Neubert,[11] N. Neufeld,[38] M. Neuner,[11] A. D. Nguyen,[39] T. D. Nguyen,[39] C. Nguyen-Mau,[39,p] V. Niess,[5] R. Niet,[9] N. Nikitin,[32] T. Nikodem,[11] D. Ninci,[23] A. Novoselov,[35] D. P. O'Hanlon,[48] A. Oblakowska-Mucha,[27] V. Obraztsov,[35] S. Ogilvy,[51] O. Okhrimenko,[44] R. Oldeman,[15,e] C. J. G. Onderwater,[67] B. Osorio Rodrigues,[1] J. M. Otalora Goicochea,[2] A. Otto,[38]

P. Owen,[53] A. Oyanguren,[66] A. Palano,[13,c] F. Palombo,[21,t] M. Palutan,[18] J. Panman,[38] A. Papanestis,[49] M. Pappagallo,[51] L. L. Pappalardo,[16,f] C. Pappenheimer,[57] C. Parkes,[54] G. Passaleva,[17] G. D. Patel,[52] M. Patel,[53] C. Patrignani,[19,i] A. Pearce,[54,49] A. Pellegrino,[41] G. Penso,[25,l] M. Pepe Altarelli,[38] S. Perazzini,[14,d] P. Perret,[5] L. Pescatore,[45] K. Petridis,[46] A. Petrolini,[19,i] M. Petruzzo,[21] E. Picatoste Olloqui,[36] B. Pietrzyk,[4] T. Pilař,[48] D. Pinci,[25] A. Pistone,[19] A. Piucci,[11] S. Playfer,[50] M. Plo Casasus,[37] T. Poikela,[38] F. Polci,[8] A. Poluektov,[48,34] I. Polyakov,[31] E. Polycarpo,[2] A. Popov,[35] D. Popov,[10,38] B. Popovici,[29] C. Potterat,[2] E. Price,[46] J. D. Price,[52] J. Prisciandaro,[39] A. Pritchard,[52] C. Prouve,[46] V. Pugatch,[44] A. Puig Navarro,[39] G. Punzi,[23,r] W. Qian,[4] R. Quagliani,[7,46] B. Rachwal,[26] J. H. Rademacker,[46] M. Rama,[23] M. S. Rangel,[2] I. Raniuk,[43] N. Rauschmayr,[38] G. Raven,[42] F. Redi,[53] S. Reichert,[54] M. M. Reid,[48] A. C. dos Reis,[1] S. Ricciardi,[49] S. Richards,[46] M. Rihl,[38] K. Rinnert,[52] V. Rives Molina,[36] P. Robbe,[7,38] A. B. Rodrigues,[1] E. Rodrigues,[54] J. A. Rodriguez Lopez,[62] P. Rodriguez Perez,[54] S. Roiser,[38] V. Romanovsky,[35] A. Romero Vidal,[37] J. W. Ronayne,[12] M. Rotondo,[22] J. Rouvinet,[39] T. Ruf,[38] P. Ruiz Valls,[66] J. J. Saborido Silva,[37] N. Sagidova,[30] P. Sail,[51] B. Saitta,[15,e] V. Salustino Guimaraes,[2] C. Sanchez Mayordomo,[66] B. Sanmartin Sedes,[37] R. Santacesaria,[25] C. Santamarina Rios,[37] M. Santimaria,[18] E. Santovetti,[24,k] A. Sarti,[18,l] C. Satriano,[25,m] A. Satta,[24] D. M. Saunders,[46] D. Savrina,[31,32] M. Schiller,[38] H. Schindler,[38] M. Schlupp,[9] M. Schmelling,[10] T. Schmelzer,[9] B. Schmidt,[38] O. Schneider,[39] A. Schopper,[38] M. Schubiger,[39] M.-H. Schune,[7] R. Schwemmer,[38] B. Sciascia,[18] A. Sciubba,[25,l] A. Semennikov,[31] N. Serra,[40] J. Serrano,[6] L. Sestini,[22] P. Seyfert,[20] M. Shapkin,[35] I. Shapoval,[16,43,f] Y. Shcheglov,[30] T. Shears,[52] L. Shekhtman,[34] V. Shevchenko,[64] A. Shires,[9] B. G. Siddi,[16] R. Silva Coutinho,[48] G. Simi,[22] M. Sirendi,[47] N. Skidmore,[46] I. Skillicorn,[51] T. Skwarnicki,[59] E. Smith,[55,49] E. Smith,[53] I. T. Smith,[50] J. Smith,[47] M. Smith,[54] H. Snoek,[41] M. D. Sokoloff,[57,38] F. J. P. Soler,[51] F. Soomro,[39] D. Souza,[46] B. Souza De Paula,[2] B. Spaan,[9] P. Spradlin,[51] S. Sridharan,[38] F. Stagni,[38] M. Stahl,[11] S. Stahl,[38] S. Stefkova,[53] O. Steinkamp,[40] O. Stenyakin,[35] S. Stevenson,[55] S. Stoica,[29] S. Stone,[59] B. Storaci,[40] S. Stracka,[23,s] M. Straticiuc,[29] U. Straumann,[40] L. Sun,[57] W. Sutcliffe,[53] K. Swientek,[27] S. Swientek,[9] V. Syropoulos,[42] M. Szczekowski,[28] P. Szczypka,[39,38] T. Szumlak,[27] S. T'Jampens,[4] A. Tayduganov,[6] T. Tekampe,[9] M. Teklishyn,[7] G. Tellarini,[16,f] F. Teubert,[38] C. Thomas,[55] E. Thomas,[38] J. van Tilburg,[41] V. Tisserand,[4] M. Tobin,[39] J. Todd,[57] S. Tolk,[42] L. Tomassetti,[16,f] D. Tonelli,[38] S. Topp-Joergensen,[55] N. Torr,[55] E. Tournefier,[4] S. Tourneur,[39] K. Trabelsi,[39] M. T. Tran,[39] M. Tresch,[40] A. Trisovic,[38] A. Tsaregorodtsev,[6] P. Tsopelas,[41] N. Tuning,[41,38] A. Ukleja,[28] A. Ustyuzhanin,[65,64] U. Uwer,[11] C. Vacca,[15,e] V. Vagnoni,[14] G. Valenti,[14] A. Vallier,[7] R. Vazquez Gomez,[18] P. Vazquez Regueiro,[37] C. Vázquez Sierra,[37] S. Vecchi,[16] J. J. Velthuis,[46] M. Veltri,[17,g] G. Veneziano,[39] M. Vesterinen,[11] B. Viaud,[7] D. Vieira,[2] M. Vieites Diaz,[37] X. Vilasis-Cardona,[36,o] A. Vollhardt,[40] D. Volyanskyy,[10] D. Voong,[46] A. Vorobyev,[30] V. Vorobyev,[34] C. Voß,[63] J. A. de Vries,[41] R. Waldi,[63] C. Wallace,[48] R. Wallace,[12] J. Walsh,[23] S. Wandernoth,[11] J. Wang,[59] D. R. Ward,[47] N. K. Watson,[45] D. Websdale,[53] A. Weiden,[40] M. Whitehead,[48] G. Wilkinson,[55,38] M. Wilkinson,[59] M. Williams,[38] M. P. Williams,[45] M. Williams,[56] T. Williams,[45] F. F. Wilson,[49] J. Wimberley,[58] J. Wishahi,[9] W. Wislicki,[28] M. Witek,[26] G. Wormser,[7] S. A. Wotton,[47] S. Wright,[47] K. Wyllie,[38] Y. Xie,[61] Z. Xu,[39] Z. Yang,[3] J. Yu,[61] X. Yuan,[34] O. Yushchenko,[35] M. Zangoli,[14] M. Zavertyaev,[10,b] L. Zhang,[3] Y. Zhang,[3] A. Zhelezov,[11] A. Zhokhov,[31] L. Zhong[3] and S. Zucchelli[14]

(LHCb Collaboration)

[1]*Centro Brasileiro de Pesquisas Físicas (CBPF), Rio de Janeiro, Brazil*
[2]*Universidade Federal do Rio de Janeiro (UFRJ), Rio de Janeiro, Brazil*
[3]*Center for High Energy Physics, Tsinghua University, Beijing, China*
[4]*LAPP, Université Savoie Mont-Blanc, CNRS/IN2P3, Annecy-Le-Vieux, France*
[5]*Clermont Université, Université Blaise Pascal, CNRS/IN2P3, LPC, Clermont-Ferrand, France*
[6]*CPPM, Aix-Marseille Université, CNRS/IN2P3, Marseille, France*
[7]*LAL, Université Paris-Sud, CNRS/IN2P3, Orsay, France*
[8]*LPNHE, Université Pierre et Marie Curie, Université Paris Diderot, CNRS/IN2P3, Paris, France*
[9]*Fakultät Physik, Technische Universität Dortmund, Dortmund, Germany*
[10]*Max-Planck-Institut für Kernphysik (MPIK), Heidelberg, Germany*
[11]*Physikalisches Institut, Ruprecht-Karls-Universität Heidelberg, Heidelberg, Germany*
[12]*School of Physics, University College Dublin, Dublin, Ireland*
[13]*Sezione INFN di Bari, Bari, Italy*
[14]*Sezione INFN di Bologna, Bologna, Italy*
[15]*Sezione INFN di Cagliari, Cagliari, Italy*
[16]*Sezione INFN di Ferrara, Ferrara, Italy*

[17]Sezione INFN di Firenze, Firenze, Italy
[18]Laboratori Nazionali dell'INFN di Frascati, Frascati, Italy
[19]Sezione INFN di Genova, Genova, Italy
[20]Sezione INFN di Milano Bicocca, Milano, Italy
[21]Sezione INFN di Milano, Milano, Italy
[22]Sezione INFN di Padova, Padova, Italy
[23]Sezione INFN di Pisa, Pisa, Italy
[24]Sezione INFN di Roma Tor Vergata, Roma, Italy
[25]Sezione INFN di Roma La Sapienza, Roma, Italy
[26]Henryk Niewodniczanski Institute of Nuclear Physics Polish Academy of Sciences, Kraków, Poland
[27]AGH - University of Science and Technology, Faculty of Physics and Applied Computer Science, Kraków, Poland
[28]National Center for Nuclear Research (NCBJ), Warsaw, Poland
[29]Horia Hulubei National Institute of Physics and Nuclear Engineering, Bucharest-Magurele, Romania
[30]Petersburg Nuclear Physics Institute (PNPI), Gatchina, Russia
[31]Institute of Theoretical and Experimental Physics (ITEP), Moscow, Russia
[32]Institute of Nuclear Physics, Moscow State University (SINP MSU), Moscow, Russia
[33]Institute for Nuclear Research of the Russian Academy of Sciences (INR RAN), Moscow, Russia
[34]Budker Institute of Nuclear Physics (SB RAS) and Novosibirsk State University, Novosibirsk, Russia
[35]Institute for High Energy Physics (IHEP), Protvino, Russia
[36]Universitat de Barcelona, Barcelona, Spain
[37]Universidad de Santiago de Compostela, Santiago de Compostela, Spain
[38]European Organization for Nuclear Research (CERN), Geneva, Switzerland
[39]Ecole Polytechnique Fédérale de Lausanne (EPFL), Lausanne, Switzerland
[40]Physik-Institut, Universität Zürich, Zürich, Switzerland
[41]Nikhef National Institute for Subatomic Physics, Amsterdam, The Netherlands
[42]Nikhef National Institute for Subatomic Physics and VU University Amsterdam, Amsterdam, The Netherlands
[43]NSC Kharkiv Institute of Physics and Technology (NSC KIPT), Kharkiv, Ukraine
[44]Institute for Nuclear Research of the National Academy of Sciences (KINR), Kyiv, Ukraine
[45]University of Birmingham, Birmingham, United Kingdom
[46]H.H. Wills Physics Laboratory, University of Bristol, Bristol, United Kingdom
[47]Cavendish Laboratory, University of Cambridge, Cambridge, United Kingdom
[48]Department of Physics, University of Warwick, Coventry, United Kingdom
[49]STFC Rutherford Appleton Laboratory, Didcot, United Kingdom
[50]School of Physics and Astronomy, University of Edinburgh, Edinburgh, United Kingdom
[51]School of Physics and Astronomy, University of Glasgow, Glasgow, United Kingdom
[52]Oliver Lodge Laboratory, University of Liverpool, Liverpool, United Kingdom
[53]Imperial College London, London, United Kingdom
[54]School of Physics and Astronomy, University of Manchester, Manchester, United Kingdom
[55]Department of Physics, University of Oxford, Oxford, United Kingdom
[56]Massachusetts Institute of Technology, Cambridge, Massachusetts, USA
[57]University of Cincinnati, Cincinnati, Ohio, USA
[58]University of Maryland, College Park, Maryland, USA
[59]Syracuse University, Syracuse, New York, USA
[60]Pontifícia Universidade Católica do Rio de Janeiro (PUC-Rio), Rio de Janeiro, Brazil (associated with Universidade Federal do Rio de Janeiro (UFRJ), Rio de Janeiro, Brazil)
[61]Institute of Particle Physics, Central China Normal University, Wuhan, Hubei, China (associated with Center for High Energy Physics, Tsinghua University, Beijing, China)
[62]Departamento de Fisica, Universidad Nacional de Colombia, Bogota, Colombia (associated with LPNHE, Université Pierre et Marie Curie, Université Paris Diderot, CNRS/IN2P3, Paris, France)
[63]Institut für Physik, Universität Rostock, Rostock, Germany (associated with Physikalisches Institut, Ruprecht-Karls-Universität Heidelberg, Heidelberg, Germany)
[64]National Research Centre Kurchatov Institute, Moscow, Russia (associated with Institute of Theoretical and Experimental Physics (ITEP), Moscow, Russia)
[65]Yandex School of Data Analysis, Moscow, Russia (associated with Institute of Theoretical and Experimental Physics (ITEP), Moscow, Russia)
[66]Instituto de Fisica Corpuscular (IFIC), Universitat de Valencia-CSIC, Valencia, Spain (associated with Universitat de Barcelona, Barcelona, Spain)
[67]Van Swinderen Institute, University of Groningen, Groningen, The Netherlands (associated with Nikhef National Institute for Subatomic Physics, Amsterdam, The Netherlands)

[†]Deceased.
[a]Also at Universidade Federal do Triângulo Mineiro (UFTM), Uberaba-MG, Brazil.
[b]Also at P. N. Lebedev Physical Institute, Russian Academy of Science (LPI RAS), Moscow, Russia.
[c]Also at Università di Bari, Bari, Italy.
[d]Also at Università di Bologna, Bologna, Italy.
[e]Also at Università di Cagliari, Cagliari, Italy.
[f]Also at Università di Ferrara, Ferrara, Italy.
[g]Also at Università di Urbino, Urbino, Italy.
[h]Also at Università di Modena e Reggio Emilia, Modena, Italy.
[i]Also at Università di Genova, Genova, Italy.
[j]Also at Università di Milano Bicocca, Milano, Italy.
[k]Also at Università di Roma Tor Vergata, Roma, Italy.
[l]Also at Università di Roma La Sapienza, Roma, Italy.
[m]Also at Università della Basilicata, Potenza, Italy.
[n]Also at AGH - University of Science and Technology, Faculty of Computer Science, Electronics and Telecommunications, Kraków, Poland.
[o]Also at LIFAELS, La Salle, Universitat Ramon Llull, Barcelona, Spain.
[p]Also at Hanoi University of Science, Hanoi, Vietnam.
[q]Also at Università di Padova, Padova, Italy.
[r]Also at Università di Pisa, Pisa, Italy.
[s]Also at Scuola Normale Superiore, Pisa, Italy.
[t]Also at Università degli Studi di Milano, Milano, Italy.
[u]Also at Politecnico di Milano, Milano, Italy.